Very Fast Hollow-Atom Decay Processes in Xe^{30+}-C_{60} Collisions

S. Martin, R. Brédy, J. Bernard, J. Désesquelles, and L. Chen

Laboratoire de Spectrométrie Ionique et Moléculaire, Université Lyon 1, UMR CNRS 5579, 43 boulevard du 11 Novembre 1918, 69622 Villeurbanne Cedex, France

(Received 1 April 2002; published 10 October 2002)

In Xe^{30+}-C_{60} collisions at low velocity (0.2 a.u. $< v <$ 0.4 a.u.), very fast electron ejection is observed not only for frontal collisions but also for near C_{60} cage collisions. In frontal collisions, the exit-charge distributions obtained with three projectile velocities are reproduced using a multistep exponential decay model. A mean Auger rate of about 0.4 a.u. is estimated for the decay of hollow atoms during the very short interaction time (< 3 fs).

DOI: 10.1103/PhysRevLett.89.183401 PACS numbers: 36.40.–c, 32.80.Hd, 34.70.+e

A slow highly charged ion (SHCI) carries a large potential energy ranging from several to hundreds of keV for $q > 15$. During its interaction with a surface or a solid, the release of that potential energy into a small target volume results in novel effects that have given rise to interests in fundamental studies on ultrafast formation and deexcitation of hollow atoms and in applications on controlled surface and material modifications [1–4]. The dynamic process during the approach and impinging of the ion on the solid has been studied intensively with x ray, with electron spectroscopy, and by analyzing the energy loss and charge of exit projectiles [5–8]. It is now well established that as the SHCI approaches the surface it becomes neutralized at a critical distance by resonant electron transfer from the target to highly excited states of the projectile as described in a ''classical over barrier'' model, leading to the formation of the so-called ''hollow atoms of the first generation'' [9–11]. The decay of such hollow atoms is very slow above the surface. Upon its impact on the surface, the electrons still in Rydberg states are ''peeled off'' and other electrons are captured to neutralize and to screen the projectile charge resulting in the formation of a more compact ''hollow atom of the second generation.'' The decay of the inner shell vacancy number of the hollow atom is described by a dynamic picture composed of ultrafast Auger transitions and continuous electron supply from the solid to the screening cloud of the hollow atom. Such a process lasts until the atomic core charge q reaches the equilibrium state q_{eq}, which is calculated using Bohr's stripping criterion, $q_{eq} = Z^{1/3} \times v$ (v in a.u.). A characteristic time of less than 10 fs has been reported for the atomic core charge decay of Au from 68+ to 1+ in SHCI-thin carbon foil (5 nm) collisions [4].

In SHCI-cluster frontal collisions [12–15], the cluster can be considered as a solid target for which the dynamic picture concerning the evolution of the projectile above and in a solid should be applied. The C_{60} fullerene is a special type of solid target with a thickness <1 nm and, as a consequence, an ultrashort transmission time in the order of a few femtoseconds for a SHCI projectile. It is then a test system sensitive to the dynamics in the ion-solid interaction during the first femtoseconds of interactions. A characteristic time of about 2 fs was found necessary for a Xe^{44+} ion to be completely screened by an electron cloud in a solid [4]. This duration is shorter than the transmission time using a 5 nm foil (7 fs), but it is comparable to the transmission time of a SHCI in a C_{60} target. On the other hand, in ion-solid collisions, the evolution of a SHCI should be attributed to sequential contributions of three interaction regimes: interaction at large distance, interaction near and above the surface, and interaction inside the solid. The contribution of short distance interaction, about several Å before penetrating the surface, is not considered in the ion-solid interaction model described above because of the shortness of this distance compared to the target thickness. However, such a distance is no longer negligible in SHCI-C_{60} collisions. Furthermore, the limited dimension of the C_{60} target allows one to study the interaction at large distance and the interaction near the C_{60} surface independently in peripheral collisions with impact parameters higher than the radius of the C_{60}, $R_0 \approx 9.5$ a.u. Meanwhile, the main difficulty using C_{60} targets for studying solidlike interaction is due to its very weak relative geometrical cross section (R_0^2/R_1^2, R_1 stands for the first electron capture distance predicted by the classical overbarrier model) which amounts to about 4% in Xe^{30+}-C_{60} collisions.

In this Letter, we report an SHCI-C_{60} collision experiment (Xe^{30+}-C_{60}) able to disentangle the three types of interaction regimes. Observations on fast electron ejection in near C_{60} cage collisions and measurements of the exit projectile charge distribution in frontal collisions provide new insight for understanding the dynamic process in SHCI-solid collisions before and after the SHCI penetrating the surface.

The experimental setup has been described elsewhere [15]. Briefly, Xe^{30+} ions intersect a C_{60} effusive vapor jet with collision energies ranging from 120 to 570 keV. The projectile final charge state $Xe^{(30-s)+}$ is selected by a cylindrical electrostatic analyzer in coincidence with the time of flight analysis of recoil ${C_{60}}^{r+}$ ions or charged fragments and the detection of the ejected electron number n_e. The ejected electrons are accelerated at 20 keV to a

semiconductor detector. The measured electron number distribution associated with each final charge $Xe^{(30-s)+}$ with s ranging from 1 to 18 allows one to get the partial cross section σ_r^s as a function of the active electron number r determined with the electron number conservation rule $r = n_e + s$. Data are presented in Fig. 1 for three collision velocities $v = 0.19$, 0.29, and 0.42 a.u.

Figure 1 provides clear evidence that the active electron number r in a single event can largely exceed the projectile initial charge ($r > 30$), which implies the ejection of a large number of electrons during the interaction time. Cross sections σ_r^s with $r > 30$ are attributed to atomlike collisions at large impact parameters ($R > R_{30}$, R_{30} being the critical distance for the transfer of the 30th electron predicted by the classical barrier model) for which the relaxation of the projectile occurs, as in ion-atom collisions, in the postcollisional process. The kinetic energy analysis of the outgoing projectile allows one to identify frontal collisions from outside C_{60} cage collisions. Typical projectile peaks obtained by scanning the electrostatic analyzer are presented in Fig. 2 for $s = 10$, 11, and 12 at $v = 0.38$ a.u. Two components attributed to outside OUT and inside IN collisions are observed for $s = 10$ and 11. The narrow "OUT" component, corresponding to a negligible energy gain, decreases in amplitude with increasing s and becomes negligible for $s \geq 12$. On the contrary, the broad "IN" component, corresponding to a mean energy loss of 1000 eV, is absent in peaks with lower s value and becomes highly predominant for $s \geq 12$. Cross sections associated with projectile IN component are then attributed to frontal collisions and drawn with grey curves in Fig. 1 ($s \geq 8$, 11, and 13 for $v = 0.42$, 0.29, and 0.19 a.u.).

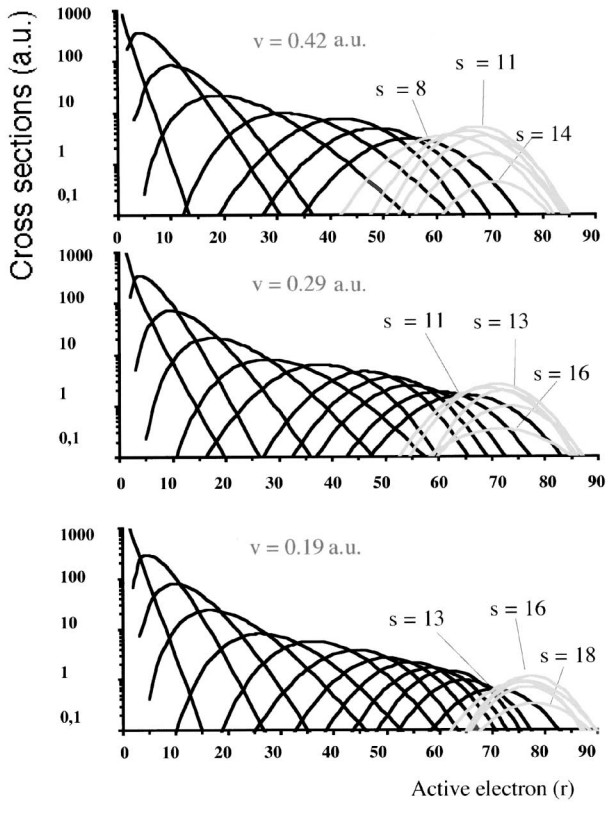

FIG. 1. Partial cross sections σ_r^s (a.u.) versus the active electron number r for each projectile final charge state $Xe^{(30-s)+}$. The corresponding s number for certain curves is indicated. Data for three projectile velocities $v = 0.19$, 0.29, and 0.42 a.u. are presented. The grey curves correspond to frontal collisions.

Cross sections with $r > 30$ and corresponding to outside C_{60} cage collisions are attributed to near C_{60} cage collisions. For $v = 0.42$ a.u., the total cross sections for atomlike, near C_{60} cage, and frontal collisions are evaluated to be 7070, 780, and 310 a.u., respectively. The corresponding impact parameter between the atomlike collision and the near C_{60} collision regimes is found to be around the critical distance for the neutralization of the projectile $R_{30} = 19$ a.u. The impact parameter between the near C_{60} and frontal collision regimes is around the radius of the C_{60} cage R_0. From Fig. 1, we can also extract the ratio between the mean active electron number $\langle r \rangle$ and the number s. For collisions at $v = 0.29$ a.u., $\langle r \rangle / s$ is found nearly constant (5–6) in both near C_{60} cage and frontal collisions. It suggests that in near C_{60} cage collisions ($R_0 < R < R_{30}$) where the SHCI does not actually penetrate the solid cage, similar dynamic picture as in SHCI-solid collisions, i.e., the formation of a more compact hollow atom and its fast decay during the collision time, should be applied. Because of the spherical symmetry of the target, we deduce that in a frontal collision the fast electron ejection process starts before the SHCI, reaching the C_{60} cage at a distance between R_{30} and R_0. The effective interaction time t for the fast electron ejection process is then estimated as $t = x/v$, where x stands for the effective interaction length limited roughly by two values, $x_{\min} = 2R_0 = 19$ a.u. and $x_{\max} = 2R_{30} = 38$ a.u.

For each projectile velocity, the projectile charge state distribution in frontal collisions is presented in Fig. 3. It is

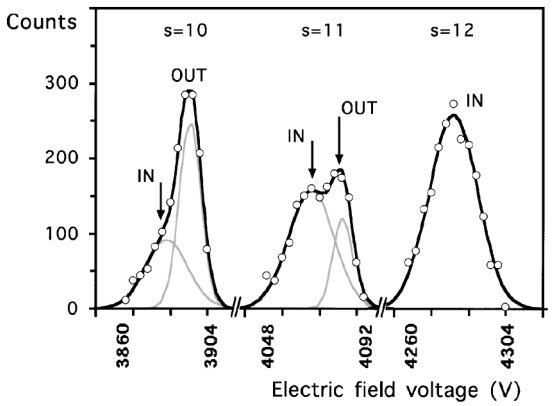

FIG. 2. Kinetic energy analyses of emerging projectile for $s = 10$, 11, and 12 ($v = 0.38$ a.u.) by scanning the electric field voltage of the electrostatic analyzer. Contributions of frontal (IN) and outside (OUT) collisions can be deduced from each peak.

noteworthy that the three distributions present similar profiles and a global shift to higher charge state is observed with increasing projectile velocity. The mean final charge states are evaluated to be 14.5, 17, and 19.5 for $v = 0.19$, 0.29, and 0.42 a.u., respectively. A similar dependency of the projectile final charge state on collision velocities, i.e., collision times, has been reported for transmitted SHCIs in a thin carbon foil (50 Å) by Hattass *et al.* [4]. The authors of the previous work have introduced a phenomenological parameter α, called equilibration rate, which is a mean deexcitation rate averaged over all atomic transitions in the course of the hollow-atom decay. In the limit case when the electron cloud built-up time is negligible, an exponential law is used to describe the final charge decay from the initial charge q_i to the equilibration charge q_{eq} as a function of the collision time, $q(t) = q_{\mathrm{eq}} + (q_i - q_{\mathrm{eq}})e^{-\alpha t}$. We employ the above exponential decay law to fit our data. The calculated final charge states are found to be 13, 17.5, and 21 for $v = 0.19$, 0.29, and 0.42 a.u., respectively, by adjusting the product αx to 3.5×10^{15} s^{-1} Å. The equilibrium rate α is found to be 1.8×10^{14} s^{-1} and 3.6×10^{14} s^{-1}, respectively, for the two limit values of interaction length $x_{\max}$ and $x_{\min}$. These values are of the same order of magnitude as that ($\alpha = 4.7 \times 10^{14}$ s^{-1}) reported for Xe^{44+} transmitted through a thin carbon foil [7].

An improved model is necessary in order to reproduce the charge state distribution for each collision velocity (Fig. 3). The approach in the following is to use a multistep cascade model [16] to describe the fast atomic core charge (q) decay of the projectile. Three assumptions are introduced. First, the population n_{q-1} for the core charge state $(q-1)+$ is supplied by the decay of the population n_q ($q \leq 30$) for the core charge state $q+$. Second, the population decay rate of each step is α_q, which is a mean deexcitation rate averaged over all atomic transition cascades of hollow atoms that occurred during the atomic core charge decay from $q+$ to $(q-1)+$. Third, the slow relaxation of hollow atoms in the postcollisional process is neglected, because of the small number of electrons stabilized in such "free region" (≈ 2 or 3). The calculated population distribution is then compared with the measured projectile final charge distribution. It seems reasonable that, when the number of active electrons in the hollow-atom decreases, the α_q equilibration rate should decrease also. In the first approximation, a linear dependency of α_q on charge q, $\alpha_q = \alpha_0(q - q_c)$, is used, so that the only free parameters in the fit are α_0 and q_c. Best fits for the three curves are obtained with $\alpha_0 = 3.7 \times 10^{14}$ s^{-1} and $q_c = 12$ as shown in Fig. 3 using the maximum effective collision length of $x_{\max} = 38$ a.u. Both the distribution profile and the mean charge value of each curve are well reproduced.

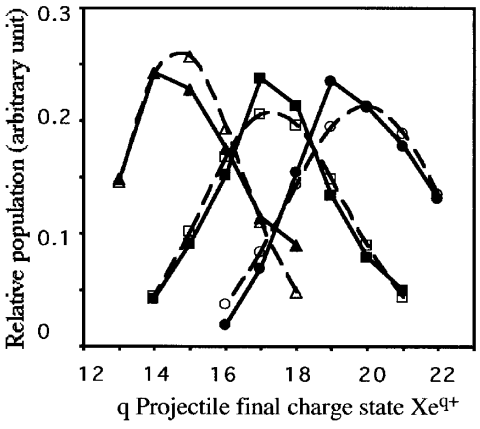

FIG. 3. Experimental and theoretical projectile charge state distributions in frontal collisions. Solid symbols (connected with solid lines): experimental data. Open symbols (connected with dashed lines): theoretical distributions obtained with the multistep cascade model. (▲, △), $v = 0.19$ a.u.; (■, □), $v = 0.29$ a.u.; (●, ○), $v = 0.42$ a.u.

Because of the linear dependency of α_q on charge q, the mean final charge state, defined as $\overline{q} = \sum_q q n_q$, is governed by the equation $d\overline{q}/dt = -\alpha_0(\overline{q} - q_c)$. It implies that the final charge state is limited by a critical value $q_c = 12$. The corresponding modified exponential decay law, $\overline{q}(t) = q_c + (q_i - q_c)e^{-\alpha_0 t}$ gives a better agreement with the experimental data. The mean final charge states are found to be 15, 17.5, and 20 for $v = 0.19$, 0.29, and 0.42 a.u., respectively. The fair agreement between the experimental data and the modified exponential model suggests that the time necessary for the formation of the second generation hollow atom should be negligible compared to the collision time, i.e., <1 fs.

It is, in fact, not astonishing that the final charge limit with a C_{60} target is much higher than the equilibration charge of a projectile in a solid. It is due to the intrinsic difference between the two targets. A solid target can be considered as a reservoir of equivalent loosely bound electrons with unlimited number, while the number of electrons in a C_{60} is limited. With decreasing atomic core charge of the projectile, the charge of the C_{60} increases, the electrons on the target are more bound, and the potential energy available on the projectile becomes lower. No more electrons can be transferred to the projectile when the ionization energy of the projectile atomic core (I_E) gets lower than that of the target. The value of the charge limit $q_c = 12$ for an incident Xe^{30+} ion can be interpreted with a simple energetic analysis. For $s = 18$ corresponding to the exit charge $q_c = 12$, the number of electrons lost by the target r is around 80 (Fig. 1). To estimate the binding energy of the 81st electron of the C_{60}, we use a linear extrapolation of the ionization energy $3r + 4$ eV from $C_{60}{}^{(r-1)+}$ to $C_{60}{}^{r+}$. The first term corresponds to the Coulomb energy necessary to remove an electron from a r-fold charged sphere to infinity. The constant term stands for the work function to take an electron out of the carbon surface, which is assumed to be independent of the charge. The obtained value, 247 eV, is effectively comparable to the ionization energy from Xe^{11+} to Xe^{12+}, $I_E(\mathrm{Xe\ XII}) = 263$ eV [17].

From Fig. 1, we can also get an idea about the mean Auger rate for the ejection of each electron. For $s = 13$, the mean active electron number $\langle r \rangle$ is found to be 70 ($v = 0.29$ a.u., Fig. 1) corresponding to the ejection of 57 electrons during an interaction time less than $t_{max} = 3.2$ fs. Under the assumption that the electrons are ejected successively, the mean time for the ejection of one electron and the mean Auger rate are estimated to be about 0.06 fs and 1.8×10^{16} s^{-1} or 0.4 a.u., respectively. However, the linear dependency of α_q on q suggests that the Auger rate is still higher at the beginning of the course of the hollow-atom decay. For example, α_{30} and α_{20} are found to be 6.7×10^{15} s^{-1} and 3.0×10^{15} s^{-1}. If we consider that the ratio $\langle r \rangle / s$ stays constant for all s values, the number of ejected electrons per stabilized electron $\langle r \rangle / s - 1$ is also constant. In the case of $v = 0.29$ a.u., on the average, 4–5 electrons should be ejected for the atomic core charge decrease of one unit. The mean Auger rate in the course of hollow-atom relaxation from $q = 30$ to 29 and from $q = 20$ to 19 can then be estimated roughly to about 3.0×10^{16} s^{-1} (0.7 a.u.) and 1.3×10^{16} s^{-1} (0.3 a.u.).

In SHCI-C_{60} collisions, according to the over barrier model, electrons are captured successively and occupy atomic orbits with the principal quantum number n ranging from 22 to 15 for the first to the 30th electron. High number of occupation a_n is found for lower n levels with $a_{12} = 8$, $a_{13} = 5$, and $a_{14} = 4$. The Auger rates of multiply excited states with the electron occupation $a_n \geq 2$ on a highly excited level n were estimated as follows [3,18,19] for an isolated atom:

$$A_{n,n'} = \frac{1}{2}(a_n^2 - a_n)\frac{5.06 \times 10^{-3}}{|\Delta n|^{3.46}} \text{ (a.u.)}. \qquad (1)$$

n' stands for the principal quantum number of the final level of the jumping electron and $\Delta n = n - n'$. In a more sophisticated calculation, Väeck and Hansen [20] found that the lifetime of the $1s7p^N$ configurations for nitrogen $N^{(6-N)+}$ decreases strongly at the neutral end of the sequence ($N = 6$). This decreasing is, in fact, due to the opening of new Auger decay channels to the limits $1s6l7p^4$, making the condition $\Delta n = 1$ possible for the jumping electron, while for configurations with lower occupation $N = 2$–5, the minimum value of Δn is 2. This behavior is general for multiply excited states with a large number of equivalent electrons.

In our case, assuming that the condition $\Delta n = 1$ is available, the Auger rates are estimated with the formula (1) to $A_{12,11} = 0.14$ a.u., $A_{13,12} = 0.05$ a.u., and $A_{14,13} = 0.03$ a.u. These values are somehow below the expected mean Auger rate of 0.4 a.u. In fact, the electrons on high Rydberg orbits are not active in the fast hollow-atom decay processes due to their low occupation numbers ($n = 15$–22; $a_n \leq 2$). At lower collision distances ($< R_{30}$), some high lying electrons can be recaptured by the target or shared by the two collision centers. It may then be possible that more electrons are transferred to lower levels, $n \leq 12$, leading to the formation of a more compact hollow atom with a higher occupation number in each level and, as a consequence, higher Auger rates. The fast ejection of one electron is followed by the capture of another one as long as the projectile stays inside or near the target. In such cases, the projectile works as an "electron pump" that makes possible the number of ejected electrons to exceed the initial projectile charge 30. As the number of fundamental vacancies decays, the number of electrons in the screening cloud decreases, leading to a decrease of the Auger rate. This is in qualitative agreement with the q dependency of the individual rate α_q and then the Auger rate. In order to get a better understanding of the fast electron ejection process, a more elaborated model is necessary. In particular, one has to take into account the electric field effect from the target and some higher order processes where several electrons are emitted simultaneously.

In summary, in frontal collisions with Xe^{30+}, the formation of a compact hollow atom starts at about 10 a.u. before penetrating the C_{60} cage and with an electron cloud built-up time shorter than the collision time (< 1 fs). A mean Auger rate of 0.4 a.u. is found necessary to interpret the fast electron ejection during the collision time. A charge limit ($q_c = 12$) in a C_{60} target is found much higher than the equilibrium charge in a solid ($q_{eq} \approx 1$).

[1] F.W. Meyer *et al.*, Phys. Rev. Lett. **67**, 723 (1991).
[2] J. P. Briand *et al.*, , Phys. Rev. Lett. **77**, 1452 (1996).
[3] J. Burgdörfer, P. Lertner, and F. Meyer, Phys. Rev. A **44**, 5674 (1991).
[4] M. Hattass *et al.*, Phys. Rev. Lett. **82**, 4795 (1999).
[5] Y. Yamazaki, Int. J. Mass Spectrom. **192**, 437 (1999).
[6] H.J. Andrä *et al.*, in *Electronic and Atomic Collisions*, edited by W.R. Mac Gillivray, IOP Conference Proceedings (Institute of Physics, Bristol, 1992), p. 89.
[7] P. Roncin *et al.*, Phys. Rev. Lett. **83**, 864 (1999).
[8] C. Lemell *et al.*, Phys. Rev. Lett. **81**, 1965 (1998).
[9] K. Tökesi *et al.*, Phys. Rev. A **61**, 020901 (2000).
[10] N. Stolterfoht *et al.*, Phys. Rev. A **61**, 052902 (2000); Phys. Rev. Lett. **88**, 133201 (2002).
[11] A. Langereis *et al.*, Phys. Rev. A **63**, 062725 (2001).
[12] J.P. Briand *et al.*, Phys. Rev. A **53**, R2925 (1996).
[13] B. Walch *et al.*, Phys. Rev. Lett. **72**, 1439 (1994).
[14] F. Chandezon *et al.*, Phys. Rev. Lett. **74**, 3784 (1995).
[15] S. Martin *et al.*, Phys. Rev. A **59**, R1734 (1999); L. Chen *et al.*, Phys. Scr. **T80**, 52 (1999); S. Martin *et al.*, Eur. Phys. J. D **12**, 27 (2000).
[16] S. M. Younger and W. L. Wiese, Phys. Rev. A **17**, 1944 (1978).
[17] R. D. Cowan, *The Theory of Atomic Structure and Spectra* (University of California Press, Berkeley, 1981), p. 13.
[18] U. Thumm, J. Phys. B **28**, 91 (1995).
[19] J. P. Desclaux, Nucl. Instrum. Methods Phys. Res., Sect. B **98**, 18 (1995).
[20] N. Veack and J. Hansen, J. Phys. B **28**, 3523 (1995).